Click-ready Iridium(III) complexes as versatile bioimaging probes for bioorthogonal metabolic labeling

Vincent Rigolot[‡], Clémence Simon[‡], Aude Bouchet, Veronica Di Battista, Dmitry Karpov, Boris Vauzeilles, Michel Sliwa, Sylvain Bohic, Christophe Biot* and Cédric Lion*

[‡] V.R. and C.S. contributed equally to this work
* corresponding authors: christophe.biot@univ-lille.fr; cedric.lion@univ-lille.fr

ABSTRACT

Herein, we report the synthesis, photophysical characterization and validation of iridium(III)-polypyridine complexes functionalized for click chemistry and bioorthogonal chemistry, as well as their versatile applications as probes in bioimaging studies exploiting metabolic labeling of intracellular glycoconjugates. The designed dyes are conjugated to chemical reporters in a specific manner within cells by CuAAC ligation and display attractive photophysical properties in the UV-visible range. They are indeed highly photostable and emit in the far-red to near-IR region with long lifetimes and large Stokes shifts. We demonstrate that they can be efficiently used to monitor nascent sialylated glycoconjugates in bioorthogonal MOE studies with a varied panel of optical and non-optical techniques, namely conventional UV-Vis laser scanning confocal microscopy (for routine purposes), UV-Vis time-resolved luminescence imaging (for specificity and facilitated multiplexing with nano-environment sensitivity), synchrotron radiation based X-ray Fluorescence nanoimaging (for high resolution, elemental mapping and quantification *in situ*) and inductively coupled plasma mass spectrometry (for routine quantification on cell populations with high statistical confidence). The synthesized Ir(III) complexes were utilized in single labeling experiments, as well as in dual click-labeling experiments utilizing two distinct monosaccharide reporters relevant to the same metabolic pathway.

INTRODUCTION

Click and bioorthogonal chemistries empower researchers to interrogate biomolecules with high selectivity and biocompatibility, utilizing pericyclic mechanisms such as the copper-catalyzed azide-alkyne [3+2] cycloaddition (CuAAC),[1] the strain-promoted azide-alkyne [3+2] cycloaddition (SPAAC),[2] or the alkene-tetrazine inverse electronic-demand [4+2] Diels-Alder cycloaddition (IEDDA).[3,4] Metabolic labeling approaches allow the introduction of bioorthogonal chemical handles into biomolecules of interest, enabling their covalent ligation with molecular dyes within living cells through such reactions. Metabolic oligosaccharide engineering (MOE), pioneered by the Reutter[5] and Bertozzi[6,7] groups, has garnered significant interest due to their pivotal role in studying glycosylation post-translational modifications (PTMs).[8] Glycosylation PTMs indeed play a crucial role in countless biological processes that involve molecular recognition (*e.g.*, cell-cell interactions, host-pathogen interactions, protein localization) and impact pathologies ranging from cancer to genetic disorders to viral and bacterial infections. Bioorthogonal chemistry is a field of chemical biology that has revolutionized the study of biological systems and continues to evolve as new reactions and chemical tools are developed and optimized.[9]

In the context of bioimaging, the rapidly advancing field of bioorthogonal chemistry still requires improvements in key aspects that can perhaps be summarized in three words: resolution, versatility, and specificity. The first of these aspects can now be enhanced through super-resolution fluorescence imaging nanoscopy, which utilizes photonic techniques in the UV-Vis range to achieve resolutions higher than those limited by the optical diffraction barrier (*ca*. 200-250 nm).[10–12] Alternatively, improvements can be made by employing techniques involving dyes that emit at much shorter and energetic wavelengths than the UV-Vis range (such as X-rays),[13] or by utilizing non-optical techniques such as cryogenic electron microscopy (cryoEM).[14] The lack of versatility is primarily due to the type of molecular probe used, which typically provides a single read-out but may not be suitable for correlative multimodal microscopy and multianalytical methods.[15] Therefore, in many research studies, bioimaging must be supplemented with additional time-consuming bioanalytical techniques that may require cell lysis, the extraction/separation of biomolecule pools and/or the use of several distinct labeling methods (*e.g.*, glycomic studies by LC-MS/MS). Finally, specificity is perhaps the main issue to tackle in many applications. Indeed, non-specific labelling may occur due to cross-reactivity of either reporters or probes with irrelevant off-target sites in the cell, or to non-covalent entrapment of unreacted dye molecules.[16] This increases non-specific fluorescence background and diminishes the specific signal-to-noise ratio, thus hampering the experiment by decreasing its sensitivity. In some cases, it might even generate aberrant false positive signals and bias the results when seeking identification of precise structures or quantification.[17]

If many efforts are constantly being made to improve bioorthogonal monosaccharide reporters and reactions in terms of specificity toward a given metabolic path, cell entry, level of incorporation, reporter group innocuity, stability or kinetics,[18–24] the most promising advances also stem from the development of improved click-ready molecular probes. For example, near-IR dyes,[25] long lifetime dyes,[26] dyes that rely on Forster's resonance energy transfer (FRET) interactions or quenching[27] or fluorogenic dyes[28] can help circumventing autofluorescence and non-specific background issues. In the search for new emissive probes to improve versatility, specificity and resolution in bioimaging studies, luminescent d^6 transition metal complexes such as iridium(III)-polypyridines are very attractive candidates. Indeed, the physico-chemical properties of d^6 metal ions and strong π-accepting ligands result in various charge transfer mechanisms that increase intersystem crossing from singlet to triplet excited states.[29–31] Thus, using UV/Vis excitation they often exhibit luminescence with long lifetimes (formally, $T_1 \rightarrow S_0$ phosphorescence as the major signal contributor) and large Stokes shifts, both exploitable aspects to improve signal-to-noise ratio and unambiguously isolate specific signals in multiple labeling experiments. The true potential of Ir(III)-based luminophores is fully realized when their lifetimes in the range of hundreds of nanoseconds to microseconds are exploited through time-resolved luminescence imaging, as this technique enables the complete elimination of the sample's short-lived autofluorescence by employing time-gated detection. As a result, the sensitivity of the experiment and the specificity of the detected signal are significantly enhanced. Moreover, in emission lifetime imaging microscopy,[32] signals originating from multiple dyes with overlapping emission spectra but differing lifetimes can be easily distinguished, thereby amplifying multiplexing capabilities. With such probes, it should be possible to utilize a single irradiation to simultaneously detect two dyes that have overlapping absorption spectra in either spectral mode or lifetime mode. In this regard, Ir(III)-polypyridine complexes present the advantage of easily modulating their photophysical parameters (absorption, emission and lifetime) when compared to other d^6 metal ions such as Ru(II), Os(II) or Re(I). In addition, iridium is practically absent from living systems and presents emission rays that do not overlap with other endogenous elements, which enables elemental mapping by X-ray fluorescence (XRF).[13] This offers an opportunity for nano-imaging with enhanced resolutions compared to optical diffraction limited confocal UV-Vis microscopy, as well as straightforward quantification by XRF or by mass spectrometry.

Although iridium(III) luminophores have been attracting much attention in the bioimaging field in the past ten years, surprisingly such probes are scarcely used to label biomolecules with bioorthogonal click chemistry.[33] Lo and co-workers, who pioneered the development of iridium sensors for bioconjugation on many application types,[29] proposed the very first proof-of-concept for phosphorescent bioorthogonal reagents to detect azide-modified biomolecules at the cell surface,

equipped with a dibenzocyclooctyne moiety for use with SPAAC labeling on living cells.[34] Highly lipophilic probes entering the cell led to strong non-specific signal and high cytotoxicity, which the authors solved by appending a carboxylate group to prevent cell entry and visualize only cell-surface glycans. The same group also developed tetrazine-based probes with luminogenic behavior after IEDDA ligations.[35–37] Focusing on spectral properties of the probes, these reports did not exploit their lifetime, and to our knowledge only two examples used time-resolved imaging so far. An iridium-alkynylbipyridine complex was described for photoluminescence lifetime imaging microscopy (PLIM) of protein pools after azido-homoalanine incorporation.[38] In this article, the lifetime of the Ir-alkyne probe was significantly shortened upon formation of the triazole cycloadduct by CuAAC, thus allowing the authors to elegantly distinguish reacted probes from unreacted probes in single-labeling experiments. More recently, a FRET-based sensing approach involving SPAAC and IEDDA was found to enable detection of caspase-3 activity with PLIM.[39]

In this work, we report the synthesis, photophysical characterization and validation of click-ready azide- and alkyne-functionalized iridium(III)-polypyridine complexes, and we showcase their potential as versatile probes in studies exploiting bioorthogonal metabolic labeling. The designed heteroleptic Ir(III) complexes are of the type $[Ir(C\wedge N)_2(N\wedge N)]^+[PF_6]^-$, in which cyclometalating 2-phenylpyridine (ppy) is the C^N backbone ligand and a phenanthroline-based N^N ligand (phen) bears a spacer arm equipped with an azide or a terminal alkyne reactive moiety. These probes are specifically conjugated to chemical reporters inside cells by CuAAC ligation and display attractive photophysical properties in the UV-visible range (*i.e.*, high photostability, large Stokes shift, long lifetime, emission in the far-red to near-IR region) and in the X-ray range. We demonstrate that they can be efficiently used to monitor nascent sialylated glycoconjugates in bioorthogonal MOE studies with a varied panel of optical and non-optical techniques (Figure 1). The synthesized Ir(III) complexes can be detected with conventional laser scanning confocal microscopy (LSCM) for routine purposes, time-resolved photoluminescence lifetime imaging microscopy (PLIM) for facilitated multiplexing and high signal specificity in multicolor settings, synchrotron radiation based X-ray Fluorescence nanoimaging (XRF-NI) for high resolution and quantitative elemental mapping, and inductively coupled plasma mass spectrometry (ICP-MS) for routine quantification on cell populations with statistical confidence. This is the first time that XRF-NI is combined to bioorthogonal chemistry to detect metabolic reporters in cells, and such data can be used correlatively with photoluminescence.
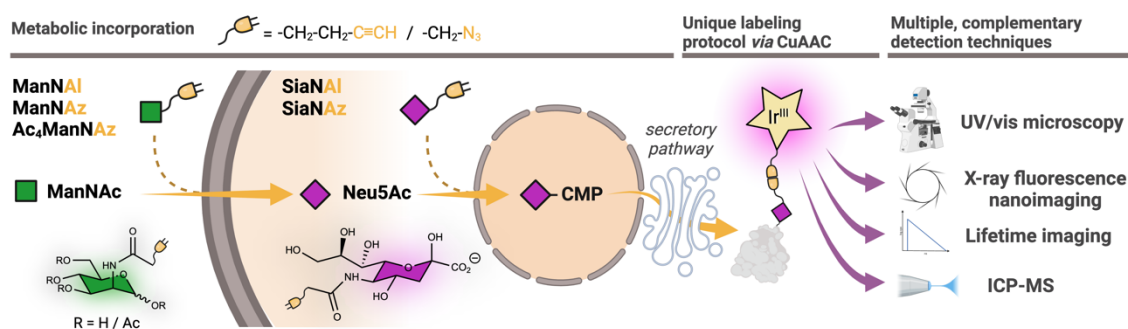
Figure 1. Chemical reporter strategy using unprotected N-acetylmannosamine (ManNAc) or N-acetylneuraminic acid (Neu5Ac) derivatives as chemical reporters and Ir(III) luminophores as molecular probes allows time-resolved PLIM bioimaging and X-ray fluorescence nanoimaging in addition routine confocal microscopy. The probes may also be used as mass tags in techniques such as ICP-MS.
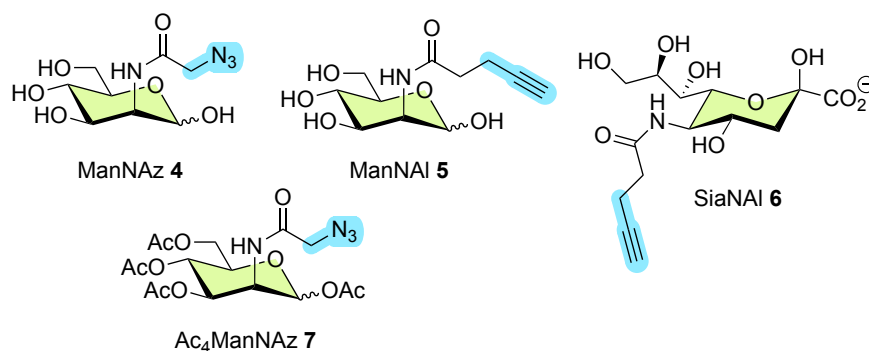
RESULTS AND DISCUSSION

Design and synthesis of click-ready iridium(III) luminophores

We envisaged *bis*-cyclometalated complexes of the $[Ir(N^\wedge C)_2(N^\wedge N)]^+$ structure family, as they are known to combine intense long-lifetime luminescence, good photostability and cell permeability while being more easily synthesized than their N_6-coordinated counterparts. The auxiliary ligand can be modified as desired to fine-tune its photophysical parameters[40] or to functionalize the complex for biological targeting[41,42] or for specific reactivity, in our case click chemistry. We thus set out to synthesize Ir(III) complexes **3a-d** with ppy as the main cyclometalating ligand, and a phenanthroline functionalized with amide-linked spacer arms and either azide or terminal alkyne reactive handles (Figure 2), in order to label sialoglycoconjugates inside cells after metabolic incorporation of modified sialic acid precursors. As opposed to the two ratiometric or fluorogenic approaches cited above, our objective here was to generate robust, versatile large Stokes shift probes with long lifetime and photophysical properties that are not influenced by the bioorthogonal reaction used for labeling. Hence, the click-reactive moiety (azide or terminal alkyne) was not designed to be conjugated to the luminophore. Owing to our previous experience in intracellular sialylation studies, we considered the introduction of a small PEG spacer arm to improve solubility and allow enough flexibility for the azide/alkyne linker to react efficiently with the metabolically engineered glycans. We opted for CuAAC as the bioorthogonal reaction, as it still remains the best candidate for detecting intracellular glycans in fixed cells in our opinion. Indeed, the potential toxicity of copper is irrelevant in this context as CuAAC ligation of the probe is carried out after cell fixation and permeabilization, while its kinetics and specificity are generally superior to SPAAC MOE approaches for intracellular applications.[16] IEDDA MOE approaches are promising[8] but still suffer from the higher steric hindrance of strained alkene reporters.
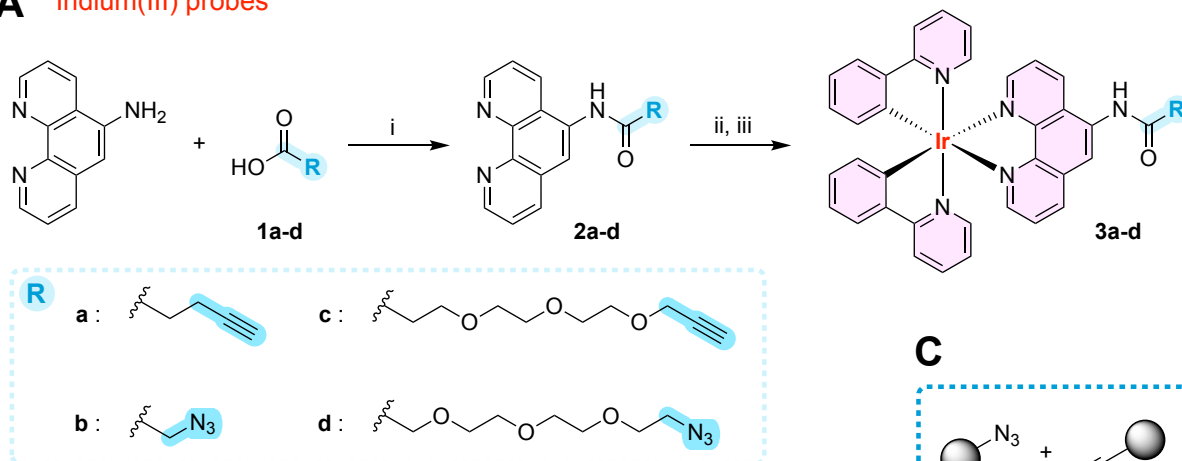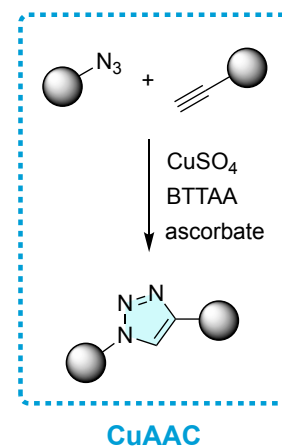
*Figure 2. A) Synthesis of Ir(III) luminophores **3a-d**. Reagents and conditions: (i) 1,10-phenanthrolin-5-amine, DCC, MeCN, rt, 20h. **2a**: 95%, **2b**: 78%, **2c**: 74%, **2d**: 72%. (ii) [IrCl(ppy)$_2$]$_2$, CH$_2$Cl$_2$/MeOH, 45 to 55°C, 5 to 15h ; (iii) NH$_4$PF$_6$, rt, 15mn. **3a**: 93%, **3b**: 54%, **3c**: 88%, **3d**: 99%. B) Structure of sialylation chemical reporters. **4, 5** and **7** are derivatives of N-Acetylmannosamine and enter the metabolic pathway at early stages in the cytosol (GNE/MNK) while SiaNAl **6** enters the pathway at the activation stage (CSS) in the nucleus. C) CuAAC allows the ligation of probes into metabolically incorporated reporters within cells.*

The synthesis of photoluminescent complexes **3a-d** and of chemical reporters *N*-azidoacetyl-D-mannosamine (ManNAz **4**), *N*-pentynoyl-D-mannosamine (ManNAl **5**) and *N*-pentynoylneuraminic acid (SiaNAl **6**) is detailed in supporting information. In brief, carboxylic acids **1a-d** were reacted with 1,10-phenanthrolin-5-amine and converted to the desired N^N bidentate auxiliary ligands **2a-d** using dicyclohexylcarbodiimide (DCC) as activating agent in acetonitrile. **1a-d** were added in a five-fold excess to compensate for the low nucleophilicity of the amine. Complexes [Ir(ppy)$_2$(phen-Alk)]$^+$[PF$_6$]$^-$ **3a**, [Ir(ppy)$_2$(phen-Az)]$^+$[PF$_6$]$^-$ **3b**, [Ir(ppy)$_2$(phen-PEG$_2$-Alk)]$^+$[PF$_6$]$^-$ **3c** and [Ir(ppy)$_2$(phen-PEG$_2$-Az)]$^+$[PF$_6$]$^-$ **3d** were obtained after reaction of two equivalents of N^N ligands **2a-d** with one equivalent of the cyclometalated dimer [IrCl(ppy)$_2$]$_2$ in CH$_2$Cl$_2$/MeOH (2:1, v/v) followed by chloride anion exchange with ammonium hexafluorophosphate. Functionalized Ir(III) complexes **3a-d** were then purified by silica

column chromatography prior to characterization by ^{1}H and ^{13}C NMR, MALDI-ToF mass spectrometry and HPLC.

Photophysical characterization

The photophysical characterization of probes **3a-d** was conducted in water and toluene in the presence or absence of oxygen, in order to measure their absorption/emission spectra and to determine their lifetimes and emission quantum yields.[43] The steady state absorption spectra of all four probes in water exhibit identical characteristics (Figures 3 and S1) and are indicative of a mixed intraligand (ILCT) and metal-ligand charge transfer (MLCT) band. They cover a broad range from 250 nm to 500 nm, with an absorbance maximum at about 260 nm, and shoulders at 375nm and at 460 nm. A broad emission spectrum (excitation at 375 nm) is measured covering the 500 to 800 nm range with a maximum at 615nm (large Stokes shift of 240 nm / 10407 cm^{-1}).

As the emission spectrum is usually assigned to a triplet excited state of ^{3}MLCT character,[44] we investigated whether the presence of oxygen might result in emission quenching. Therefore, the quantum yields (Φ) and lifetimes (τ) of **3a-d** were measured in both aerobic and degassed conditions (Figures S2 and S3). The literature also documented the potential impact of polarity, leading us to determine these photophysical properties in toluene as well as in aqueous media.

In water, the quantum yields (Φ) were measured at about 3-4%, (Table 1), reasonable values corresponding to those previously described in the literature for similar structures (*i.e.* about 1-2%),[35,36,45] and the emission lifetimes were revealed to be quite insensitive to oxygen. The emission decay τ in water is monoexponential with an average lifetime of *ca*. 70-80 ns. Interestingly, the lifetime in toluene was found to be longer and strongly dependent on the presence of oxygen. In degassed conditions, τ was indeed measured at *ca*. 700 ns, a 7-fold increase when compared to the value in aerobic conditions (*ca*. 100 ns). These results point out the sensitivity of the triplet excited state to polar environments as well as to oxygen. On average, probes **3c** and **3d** bearing a PEG$_3$ spacer arm were found to have slightly larger τ values (ca. 15%) than probes equipped with a shorter, more hydrophobic alkyl spacer arm **3a** and **3b**. In cell labeling experiments (Figures S11-S13), the obtained signal comprises two components: a fast lifetime (< 5 ns) corresponding to cell autofluorescence, and a long lifetime corresponding to the Ir(III) complex. The long lifetime of **3c** and **3d** (*ca*. 400 ns) was consistently found to be longer in cells than in non-degassed solutions, in between the value obtained in solution for aerobic conditions and the value in degassed toluene. This τ value is homogeneous across the cell, regardless of the localization. The complex heterogeneous polarity microenvironments in cells may shield the triplet excited states from the effect of water thus leading to longer average lifetimes when compared to experiments in aqueous solutions, particularly when considering that the tagged *N*-glycoconjugates are majoritarily anchored in hydrophobic membranes. In addition, the fact

that an anti-oxidant anti-fading mounting medium is used for imaging experiments might also aid in averting quenching and contribute to lengthening the lifetime of Ir(III) dyes.
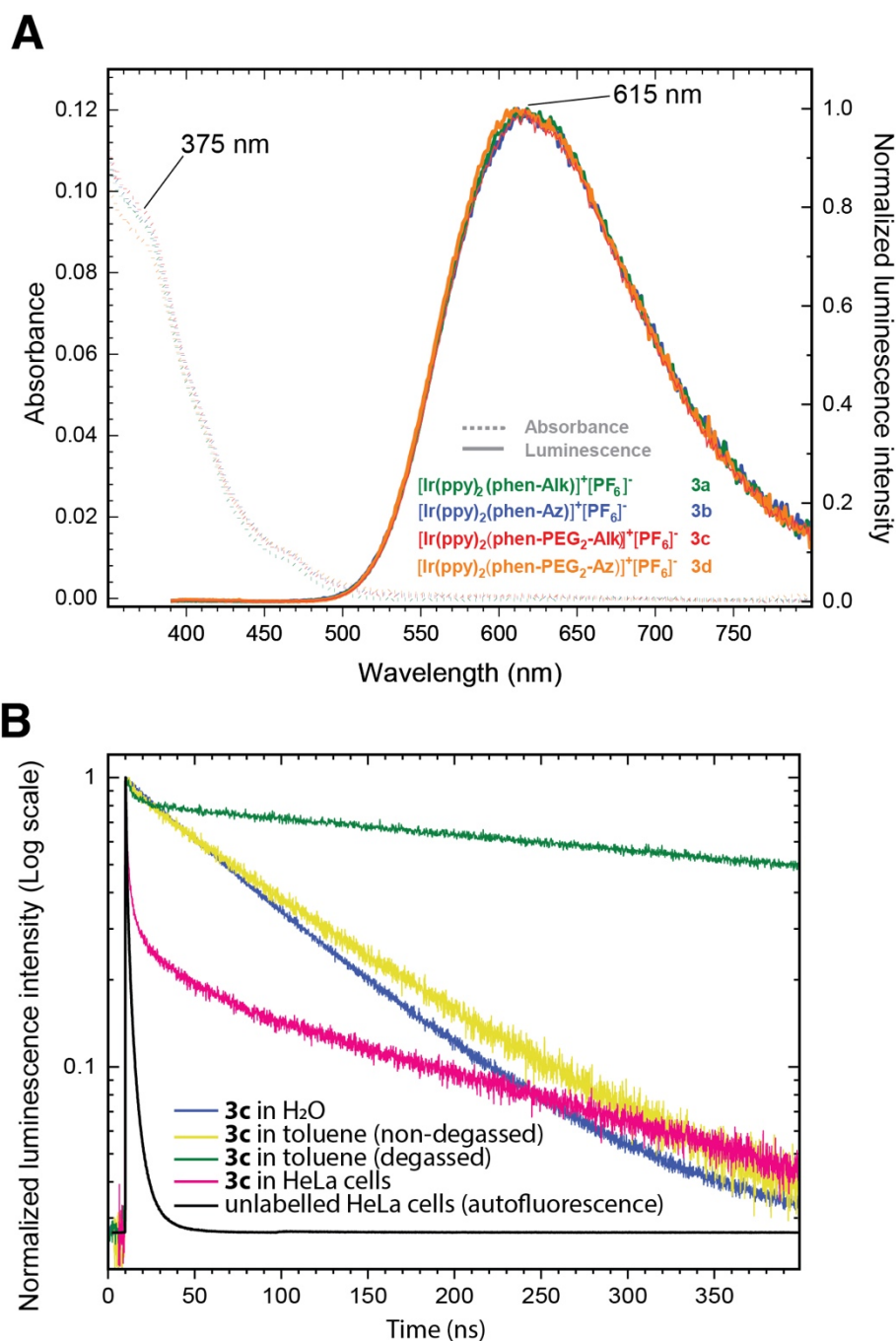

*Figure 3. A) Absorbance (dashed line) and normalized luminescence upon excitation at 375 nm (solid line) of probes **3a-d** in water. B) Emission decay at 375 nm excitation for **3c** in water and toluene (non-degassed and degassed by bubbling argon), and in cells, versus emission decay of cell autofluorescence. Note: the decay in cells presents a fast component due to cell autofluorescence and a long component due to the Ir(III) probe.*

	τ_{av} H₂O	τ_{av} H₂O degassed	τ_{av} toluene	τ_{av} toluene degassed	τ_{av} in cells	Φ H₂O
3a	68.8 ± 0.2 ns	71.4 ± 0.3 ns	98.7 ± 0.3 ns	728.0 ± 0.6 ns	-	3.8%
3b	67.8 ± 0.2 ns	68.9 ± 0.3 ns	88.7 ± 0.2 ns	454.4 ± 0.7 ns	-	3.4%
3c	81.9 ± 0.2 ns	79.7 ± 0.3 ns	98.9 ± 0.4 ns	744.6 ± 0.5 ns	369.5 ± 2.8 ns	3.9%
3d	76.0 ± 0.2 ns	74.2 ± 0.3 ns	93.8 ± 0.2 ns	696.2 ± 0.9 ns	401.7 ± 12 ns	4.0%

*Table 1. Average luminescence lifetimes τ_{av} of probes **3a-d** under excitation at 375 nm in water ($\lambda_{em} = 600$ nm) and in toluene ($\lambda_{em} > 500$ nm) for aerobic and degassed solutions, and in cells ($\lambda_{em} > 500$ nm). Quantum yields Φ of probes **3a-d** in aerobic water.*

Probe validation *in vitro*

We then investigated whether probes **3a-d** could be efficiently conjugated by CuAAC to adequately functionalized monosaccharides in aqueous medium, in conditions relevant to bioorthogonal cellular assays.[46] All four probes were reacted with a corresponding sugar reporter, namely either ManNAz **4** or ManNAl **5**. The CuAAC ligations were monitored by HPLC equipped with UV and fluorescence detectors (Figures S4-S5), and the formed cycloadducts were characterized by MALDI-ToF mass spectrometry of the isolated HPLC fractions (Figure S6). PEGylated probes **3c** and **3d** were quickly and fully converted to the desired cycloadducts as expected, indicating fast kinetics suitable for cell culture experiments. However, we observed that the reaction of probes **3a** and **3b** was significantly advanced but still incomplete after two hours, showing conversion rates of 94.5% and 77.5%, respectively. The reactivity assessed in aqueous solutions with a monosaccharide does not directly translate to the reactivity of probes reacting in the midst of cells, which are composed of a multitude of complex heterogeneous microenvironments with highly variable hydrophobic-hydrophilic balances, and the local concentration of reporter subunits is not uniform throughout the cell. However, this result hinted at a potentially lesser labelling efficiency for dyes **3a** and **3b** in subsequent biological experiments than for **3c** and **3d**.

Metabolic labeling of sialoglycoconjugates in cells

The probes were then incorporated in HeLa cells to monitor the biosynthesis of sialylated glycoconjugates by MOE and observed in laser scanning confocal microscopy. Sialic acids, a diverse group of monosaccharides, are found at the non-reducing ends of glycan chains of glycoproteins and glycolipids. Entering the sialic acid metabolic pathway, ManNAz **4** and ManNAl **5** are intracellularly converted in three steps to the corresponding azide- and alkyne-tagged sialic acids, respectively, then incorporated into nascent sialoconjugates in the Golgi apparatus after being activated as cytidine monophosphate nucleotide sugars in the nucleus. During its life cycle, the formed sialoconjugates are

then generally exported to the cell membrane via the secretory pathway, and can be re-internalized during pinocytosis and recycled.[46]

Cells incubated with ManNAz **4** were reacted with alkyne-functionalized [Ir(ppy)$_2$(phen-Alk)]$^+$[PF$_6$]$^-$ **3a** or [Ir(ppy)$_2$(phen-PEG$_2$-Alk)]$^+$[PF$_6$]$^-$ **3c** using the copper sulfate / ascorbate catalytic system in the presence of copper tetravalent ligand BTTAA, adapting our previous protocol, while cells incubated with ManNAl **5** were labeled with azide dyes [Ir(ppy)$_2$(phen-Az)]$^+$[PF$_6$]$^-$ **3b** or [Ir(ppy)$_2$(phen-PEG$_2$-Az)]$^+$[PF$_6$]$^-$ **3d**. Iridium probe concentration, reporter incubation time and CuAAC parameters were optimized for maximum signal-to-noise ratio (Figures S7-S8-S9).

 Azide **3a** and alkyne **3b** at concentrations ranging from 1 to 100 μM did not lead to efficient marking of sialylated structures (Figure 4). Although HPLC monitoring of the reaction in solution indicated a slower but decent rate, we had expected these probes to bind to sugar reporters in cells. An analogous Ir-alkyne complex with no spacer arm was indeed previously reported to bind to azide-tagged protein pools after incubating cells with 2 mM azidohomoalanine in methionine-depleted medium.[38] However, in our case the non-specific background signal was consistently too high to detect any potential specific labeling. The short, rigid spacer arms of **3a** and **3b** combined to the hydrophobic nature of the complex core might not confer enough flexibility for the reactive handle to efficiently access reporter groups in the highly polar microenvironment of glycan chains. The issue might also stem from the low incorporation rate of monosaccharide reporters that leads to a lower concentration of tagged biomolecules in MOE than for residue-specific protein labeling.

Conversely, probes **3c** and **3d** bearing a flexible PEG$_3$ spacer arm capable of accepting hydrogen bonds provided images with efficient and highly specific labeling when compared to negative control conditions (Figure 4). The obtained pattern is fully consistent with intracellular sialylation studies previously evidenced with small organic fluorophores such as click-reactive tetramethylrhodamines (TAMRA).[46,47] Alkyne-functionalized probe **3c** was selected for further studies.
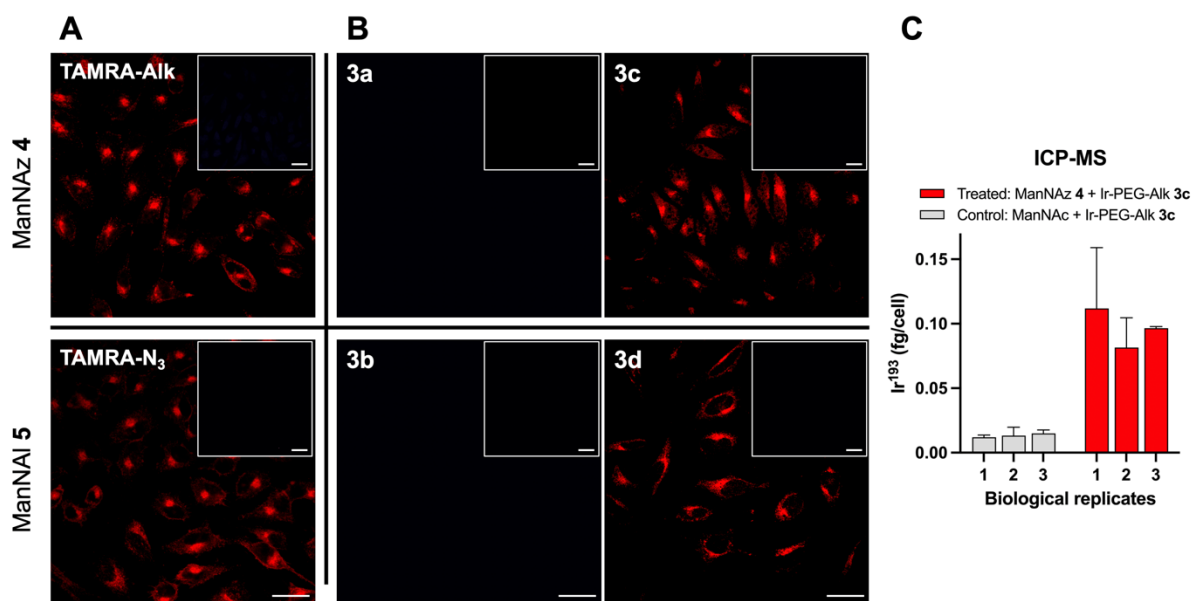
*Figure 4. Bioorthogonal labeling of sialoglycoconjugates with Ir(III)-ppy complexes observed by laser scanning confocal microscopy. Cells were incubated with ManNAz **4** (top) or ManNAl **5** (bottom) and reacted with complementary probes: **(A)** TAMRA-N₃ or TAMRA-Alk ; **(B)** probes **3a-d**. A negative control showing cells reacted with each probe after incubation of untagged N-acetylmannosamine (no chemical reporter) is shown in the top-right corner of each image. (C) ICP-MS analysis of cells reacted with **3c** after incubation with ManNAc (control, grey) or ManNAz (reporter, red). Quantity of incorporated iridium is reported in ng per cell. Experiments were carried out as three biological replicates and two technical measures on each replicate. Scale bar = 30μm.*

ICP-MS quantitative analysis *in cellulo*

We went on to check whether these bioorthogonal probes could facilitate the quantification of reporters metabolized into cell glycoconjugates with ICP-MS. Given its low abundance in nature, iridium is characterized by a very low limit of detection (0.001 to 0.01 ppb), a clear benefit when considering that the rate of incorporation of monosaccharides in neo-formed glycoconjugates has been reported to be quite poor (*ca.* 5%). Cells were incubated with ManNAz **4** (or ManNAc as control) and labeled with **3c** after cell fixation and permeabilization. A thorough washing procedure was optimized to eliminate the excess reactant as well as the pool of soluble metabolic intermediates prior to acidolysis. On average, the amount of iridium was found to be 7.3-fold higher in samples treated with ManNAz than in the control (Figure 4C and Table S1), illustrating the potential of such bulk quantitative analysis to complement photoluminescence imaging data.

Ir(III) complexes photostability

The photobleaching of **3c** was then assessed and compared to two dyes reputed for their photostability (Figure 5). In cells incubated with either ManNAz **4** and labeled with either **3c**, or with ManNAl **5** and labeled with Alexa Fluor 405-Azide, 108 x 108 μm squares (512 pixels x 512 pixels) corresponding to a

single cell were continuously scanned with laser irradiation at 405 nm with a dwell time of 50 µs/pixel in the presence and absence of antifade reagent. **3c** was revealed to be remarkably photostable and robust, with 85% of the mean photoluminescence intensity being retained after 80 seconds of exposure to the laser, time by which Alexa Fluor 405 was fully photobleached. Dye **3c** excited at 405 nm even proved to be more photostable than Alexa Fluor 488 excited at the lower energetic wavelength 488 nm (Figure S10). Susceptibility to hydrolysis was also tested in PBS buffer over several weeks and no degradation was observed. Altogether the designed probes displayed consistent photophysical parameters independent of the bioorthogonal handle used, with large Stokes shift and long emission lifetime, and are chemically robust and highly photostable. They are thus ideal candidates for applications in multicolor time-gated bioimaging, whereby luminophores are distinguished using differing time ranges (Δt) of photon emission after an excitation pulse.
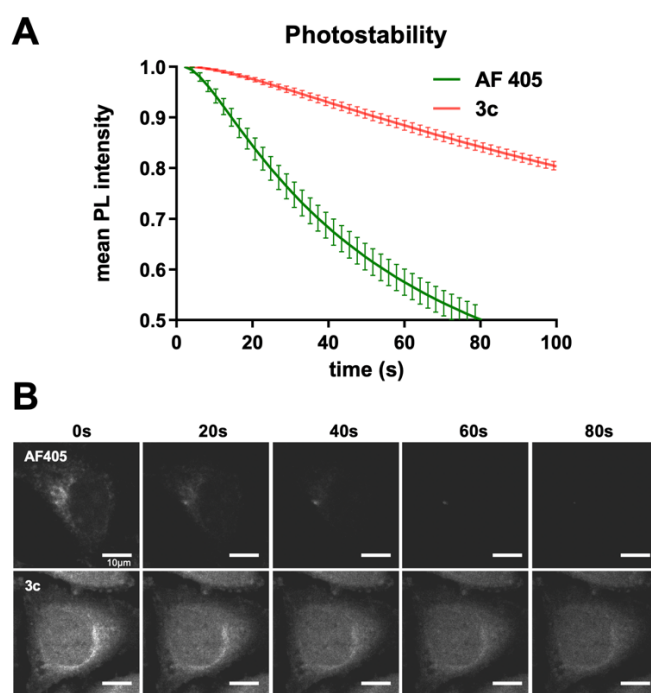

*Figure 5. Photostability of probe **3c** compared to Alexa Fluor 405-Azide. The probes were linked to reporter units by CuAAC after metabolic incorporation of ManNAz **4** or SiaNAl **6**, respectively, in HeLa cells for 48h. **(A)** mean photoluminescence (PL) intensity of confocal images (108x108µm, 211nm px size, 2s per image). Three technical replicates were measured. **(B)** confocal images of a single cell monitored during continuous data acquisition (35x35µm, 211nm px size). Excitation: 405 nm. Emission detection filter: bandpass 450/50 nm for AF405, longpass >600 nm for **3c**.*

Time-resolved Photoluminescence Imaging Microscopy

We then investigated Ir(III) complexes in lifetime imaging, using a single laser excitation pulse to distinguish two probes in time-gated experiments. Classical methods based on spectral properties

acquire several images with different sets of excitation light and emission filters to separate probes which emit in different regions and/or can be excited at different wavelengths. In contrast, in time-gated emission methods, imaging of different marking patterns can be obtained in one experiment using a single excitation pulse, thus reducing photobleaching and any optical artefact that could occur changing the irradiation/detection conditions, improving temporal resolution, as well as enhancing multiplexing capabilities.

Firstly, dual labeling experiments were conducted with **4/3c** and DAPI. In this context, the two probes are not localized in the same region of the cell: at the incubation time used for **4**, **3c** (long lifetime) is conjugated upon bioorthogonal ligation to nascent sialoconjugates that are mainly localized in the Golgi apparatus, with a less intense secondary pool at the cell membrane. In contrast, DAPI (short lifetime, τ = 2 ns)[48] is well-known to localize in the nucleus upon binding with the minor groove of DNA, thus providing a straightforward platform to validate signal specificity in single pulse time-gated experiments (Figure 6). Images of labeled HeLa cells were acquired on an in-house designed microscope using a 405 nm picosecond pulsed laser excitation and a long-pass filter, to collect all photons with a wavelength superior to 500 nm with an avalanche photodiode-based single-photon counting detector. The experimental setup used for this "1-color/2-probes" approach and the negative control samples are shown in supporting information (Figure S14). Time-gating was then applied to unmix emitted photons corresponding to DAPI (blue channel, photons arrival time Δt < 20 ns) and to sialoglycoconjugates (40 < Δt < 500 ns).
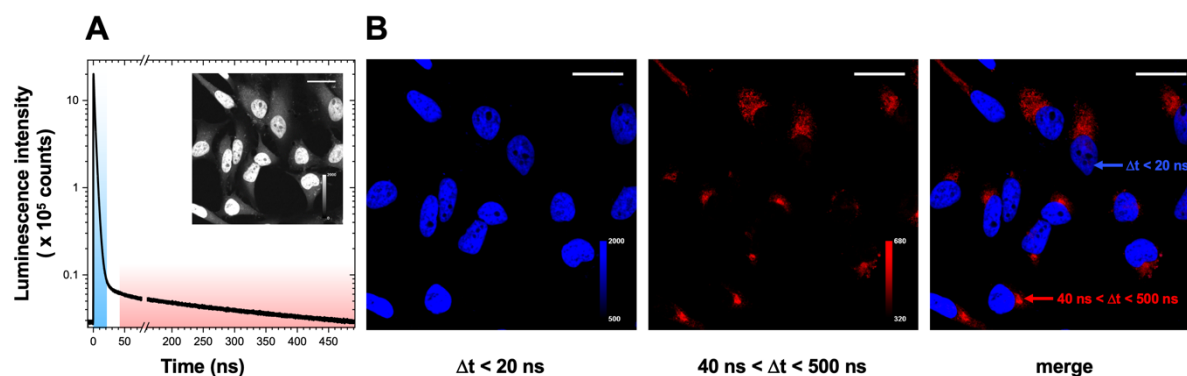
*Figure 6. HeLa cells labeled with ManNAz **4** / Iridium complex **3c** (sialoconjugates) and DAPI (nucleus). A) Emission time decay and raw image with all collected photons used to generate time-gated channels. Excitation at 405 nm and detection with long pass filter > 500 nm. B) Time-gated images for early photon arrival times in blue (Δt < 20 ns, left), late photon arrival times in red (40 < Δt < 500 ns, middle), and merge of the two channels (right). The marking patterns are typical of DAPI and of sialylated glycoconjugates, respectively. Experiments were carried out as three biological replicates. Scale bar = 30 µm.*

These results clearly demonstrate the ability of such Ir(III) complexes to be exploited in multicolor imaging to generate highly specific channels. We then showed the full potential of probe **3c** in dual labeling experiments exploiting two monosaccharide reporters of the same metabolic pathway. For that purpose, we used ManNAz **4** and SiaNAl **6**, as they are indeed both incorporated as sialic acid units in glycoconjugates, but enter the metabolic network at two different points. SiaNAl **6** enters cells by pinocytosis and is directly activated in the nucleus as the sugar nucleotide donor cytidine 5'-monophospho *N*-pentynoylneuraminic (CMP-SiaNAl) acid prior to Golgi export and transfer onto a nascent glycoconjugate by a sialyltransferase. ManNAz **4** must follow a longer path as it penetrates cells through a yet unknown transport mechanism and undergoes three enzymatic conversions in the cytosol (phosphorylation to ManNAz-6-P, conversion to SiaNAz-9-P by condensation with phosphoenolpyruvate, then dephosphorylation to SiaNAz) before it can be transported to the nucleus and activated as CMP-SiaNAz.[46] Therefore, the reporters are expected to be localized in the same regions of the cell, but with different kinetics of incorporation.

Hela cells incubated with both reporters were submitted to two consecutive CuAAC labeling steps. ManNAz **4** was reacted with long-lifetime alkyne dye **3c**, while SiaNAl **6** was ligated to short-lifetime Alexa Fluor 405-Azide. Cells were then imaged as described above (Figure 7). Using similar time-gating analysis, we could get an image specific of Alexa Fluor 405 (green channel) and of **3c** (red channel), with full signal specificity of each channel and with no need for fitting the time-dependent signal. To the best of our knowledge, this is the first time that both a sialic acid reporter and a *N*-acetylmannosamine reporter are used simultaneously in the same cell to generate dual color maps of intracellular sialylation. Partial co-localization of time-resolved signals was observed, but as expected some signals are not co-localized, thus evidencing differences in metabolism kinetics between the two reporters. This dual-labelling method could provide a useful imaging platform in the future for studying the early steps of sialylation pathways, or for investigating trafficking and recycling of sialoconjugates in pathologies such as congenital disorders of glycosylation (CDGs).
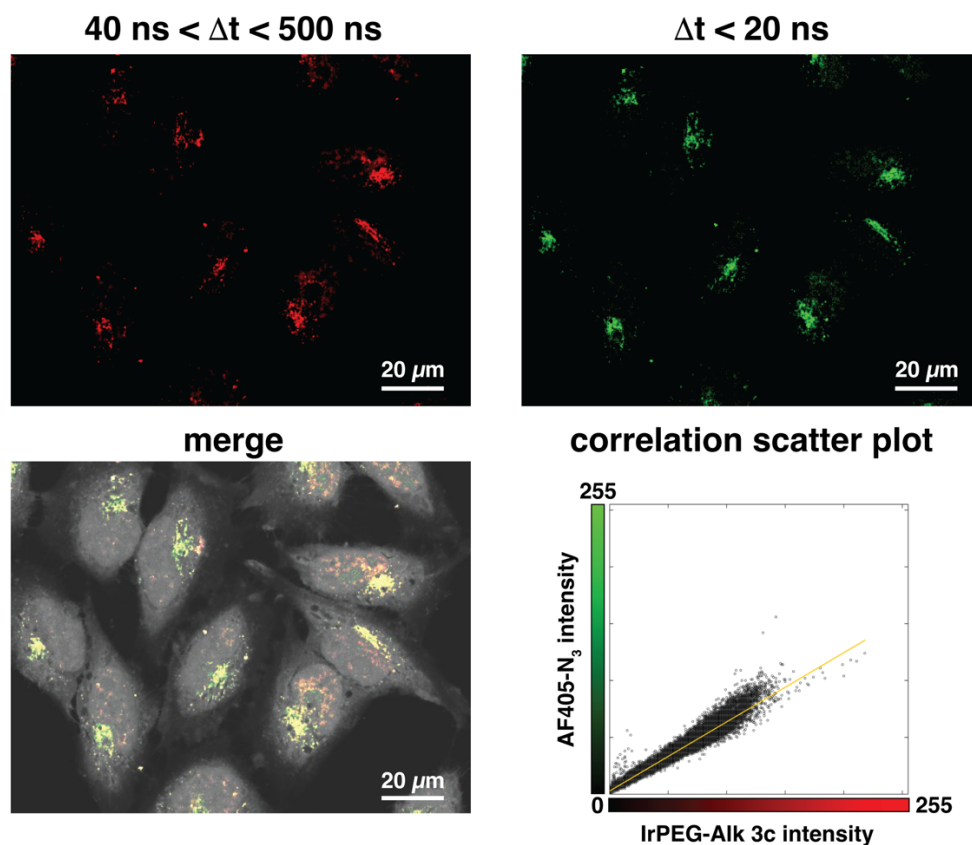
*Figure 7. Time-resolved imaging of HeLa cells dual labeled with SiaNAl **6** / Alexa Fluor 405-Azide and with ManNAz **4** / Ir(III) dye **3c**. Top left: time-gated channel showing photons emitted between 40 and 500 ns after the excitation pulse (specific of **3c**). Top right: time-gated channel showing photons emitted between 0 and 20 ns after the excitation pulse (specific of Alexa Fluor 405). Bottom left: merge image showing both long (**3c**, red) and short (AF405, green) lifetime signals, overlayed with an image showing the raw full photon count (grey). The levels of the grey channel are not adjusted to the negative control in order to outline the cells. Bottom right: correlation scatter plot of the red (**3c**) and green (**AF405**) channels. Excitation at 405 nm and detection with long pass filter > 410 nm. Experiments were carried out as three biological replicates.*

Additional time-resolved experiments using a more conventional set-up using two excitation pulses at two different wavelengths to separately acquire the two channels were also successfully performed. In these experiments, ManNAz **4** and SiaNAl **6** were bioorthogonally labeled with **3c** and AlexaFluor 488, respectively (Figure S15). The advantages of clickable Ir(III) probes in multiplexed settings are further showcased here: although the emission spectra of **3c** and of AlexaFluor 488 partially overlap, as well as their absorption spectra, time-gating allows unambiguous distinction of the photon's origin (*i.e.*, from which probe it was emitted), ensuring high confidence on the signal specificity of each channel.

Synchrotron-radiation based X-ray Fluorescence nanoimaging

While optical microscopy is the method of choice for imaging labeled biomolecules within the context of a living cell, X-ray fluorescence nanoimaging (XRF-NI) techniques developed at some synchrotron facilities provide a highly complementary subset of information. Indeed, XRF-NI now allows high-spatial resolution (30-50 nm) of the detected elements within a sub-cellular structure combined to a high degree of sensitivity, as shown for Zn in neuronal structures reaching a very low limit of detection of 130 atoms of zinc within a 40 nm pixel size.[49] In addition, unlike most optical methods, XRF-NI provides absolute quantification through elemental composition mapping of the cell. Despite the low-throughput nature of the technique due to low temporal resolution, these benefits are great assets in the quest for quantifying intracellular metabolic probes that are expected to report locally for a very low number of molecules at the nanoscale.

In our context, achieving optimal results entails the development of adequately designed click-reactive XRF sensitive probes such as **3c-d** for quantitative subcellular mapping purposes. Iridium is indeed an ideal candidate for nanoscale XRF-NI, having no biological role and an extremely low abundance in living organisms (below 1 ng/L in serum for example).[50] Thus, endogenous Ir is not detected by XRF within cells and does not induce any X-ray autofluorescence background. Furthermore, main X-ray fluorescence emission rays can be observed for Ir at 9.175 keV (Lα) and 10.708 keV (Lβ), a region nearly devoid of emission lines from biologically important elements observed in cells. This ensures a minimal background signal and provides clear and accurate results without interference from other cellular components. In our samples, only the Zn-Kβ X-ray emission line at 9.57 keV is situated close to the Ir-Lα emission line, while the Ir-Lβ line is in a spectral region completely free of other element contribution. Spectral fitting with a dedicated software allows the deconvolution of any potential spectral overlap as well as the removal of any background contributions, to get the net peak area for all elements detected. From these, a local concentration can be calculated for each pixel using the fundamental parameter method as already reported in similar XRF-NI studies (see SI for details).[13,51]

To illustrate the capabilities of clickable Ir(III) dyes in XRF-NI, we explored their potential in distinguishing labeling patterns derived from two widely employed reporters for studying sialylation, namely per-O acetylated Ac$_4$ManNAz **7** and free-hydroxyl ManNAz **4**. Whereas per-*O*-acetylated monosaccharides are commonly used in mammalian models, it has been shown that per-*O*-acetylation generates non-specific signal and false positives.[21] It may also lead to metabolic perturbation due to partially acetylated forms, thus for reporters that are capable of entering cells by active transport such

as ManNAc or Sia derivatives, we tend to prefer unprotected reporters in studies aimed at investigating intracellular metabolic paths.[16] HeLa cells were grown for 48h on graphene-coated silicon nitride membranes with either ManNAz **4**, Ac$_4$ManNAz **7** or ManNAc as control and submitted to CuAAC with **3c** as described hereabove. The labeled cells were first observed by confocal fluorescence microscopy in PBS with an immersion objective to minimize any damages to the cells and/or the Si$_3$N$_4$ membranes. This allowed us to capture wide field images and to observe every cell on each membrane prior to XRF experiments at the synchrotron. Cells were kept under PBS at 4°C until they were quickly rinsed with an ammonium acetate buffer, vitrified by plunge-freezing in liquid ethane and kept under liquid nitrogen before cryo-transfer for cryo-XRF nanoimaging.[52] In the present case, the sample analysis at cryogenic temperature limits the impact of the intense focused X-ray beam and radiation damages on cells during acquisition of XRF data.[53]

The online transmitted light microscope allowed us to precisely select the cells of interest and generate a direct comparison between confocal UV/vis phosphorescence and XRF images (Figure 8 and S17). We observed a strong correlation between both experiments, with clear co-localization of the probes by UV/vis phosphorescence and the iridium XRF signal. While the UV/vis signal is fainter and blurrier, cryo-XRF allows much finer details to be observed, which is especially visible in the ManNAz condition where a punctiform pattern around the Golgi apparatus is revealed (Figure 8A, 8C). A slightly different labeling profile is observed with the free-hydroxyles reporter ManNAz **4** compared to the peracetylated Ac$_4$ManNAz **7**, for which the pattern seems more diffuse and scattered, possibly due to partial non-specific incorporation of the reporter,[18,21] or to a lower rate of incorporation at this incubation time point. XRF-NI experiments give access to the Iridium surface mass expressed in ng/mm^2 which, combined with surface measurements, allows us to precisely determine the quantity of Iridium atoms and thus the number of probe molecules bound within the cells for each condition analyzed. In multimodal approaches, XRF-NI combined with UV-Vis luminescence microscopy may thus be used to link the arbitrary luminescence units to actual quantitative values in future studies. Incidentally, in the incubation conditions used here (48h for both sugars in HeLa cells), the surface density of Ir(III) probe was shown to be higher after ManNAz incubation than after Ac$_4$ManNAz incubation (Figure 8B), an unexpected result confirming that unprotected ManNAz has a high potential as sialylation reporter, as it avoids most of the non-specific labeling caused by peracetylated reporters. Indeed, whereas incorporation of peracetylated reporters is usually thought to be more efficient than free-hydroxyl reporters because they enter cells by passive diffusion, they need to undergo full deacetylation through the action of non-specific esterases in order to release the free metabolite. In our case, their actual metabolic incorporation in glycoconjugates was less efficient. While detection of iridium probe **3c** by ICP-MS allows bulk statistical analysis on a large pool of cells (Figure 4C), its use in XRF-NI thus provides much finer analysis through iridium mapping as it retains subcellular spatial

information with high resolution and sensitivity. Combined with photoluminescence techniques, such clickable organometallic complexes are thus versatile tools that may allow in-depth investigation of sialylation metabolism in pathological contexts.
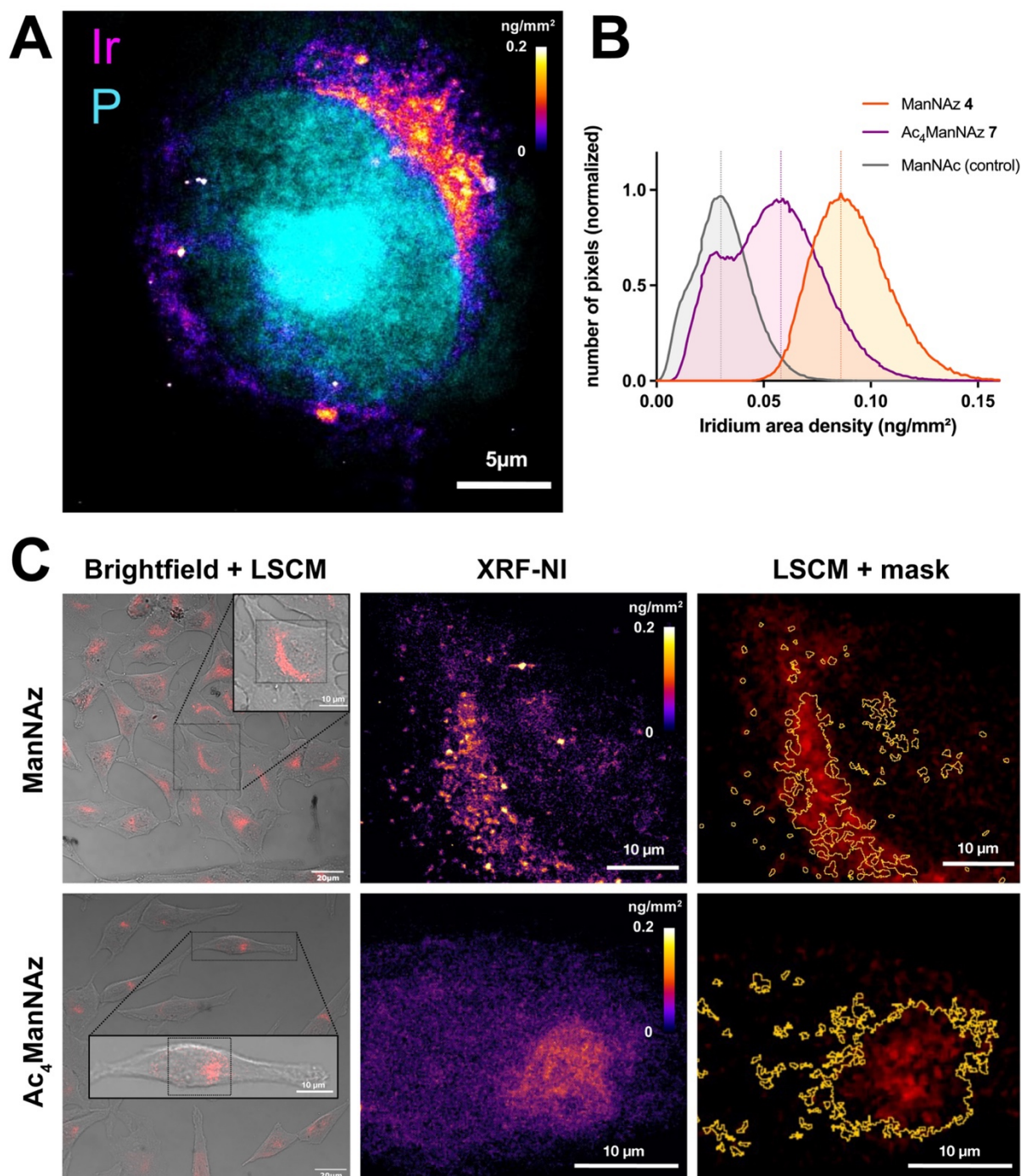

Figure 8. *X-ray fluorescence nanoimaging (XRF-NI).* ***(A)*** *XRF elemental imaging of Iridium (fire colorscale,* ***3c****) and Phosphorus (cyan, nucleus) in HeLa cell after 48h ManNAz* ***4*** *incorporation shows 16-fold improved resolution compared to UV/vis confocal microscopy (50nm/px).* ***(B)*** *Comparison of*

*Iridium area density (ng/mm²) in XRF analyzed cells after incorporation of ManNAz **4** (orange), Ac₄ManNAz **7** (purple) or ManNAc (grey, control) followed by CuAAC conjugation of **3c**. Three replicates were measured. **(C)** Bimodal observation of HeLa cells after incorporation of ManNAz **4** (Top) or Ac₄ManNAz **7** (Bottom) and CuAAC labeling with **3c**. Cells were observed by laser scanning confocal microscopy (left, brightfield + **3c** UV/Vis photoluminescence) and analyzed with cryo-XRF-NI (middle). XRF-NI analysis allowed the creation of masks showing great correlation between UV/vis and XRF signal and improved sensitivity (right). Curves with SD are shown in Fig. S17, Negative control images are shown in supporting information.*

CONCLUSION

In this work, click-ready Ir(III)-polypyridine complexes were synthesized, characterized and applied as bioimaging probes in metabolic labeling studies. These tools displayed remarkable photophysical properties, and were shown to offer clear benefits terms of resolution, specificity or sensitivity using various techniques such as laser scanning confocal microscopy, time-resolved photoluminescence lifetime imaging, inductively coupled plasma mass spectrometry and X-ray fluorescence nanoimaging. They allowed dual imaging of two chemical reporters of the sialylation pathway with a single excitation pulse in time-gated experiments, which paves the way for future studies focusing on the kinetics and dynamics of sialoconjugate metabolism and trafficking in pathological vs. physiological contexts. They also led to high-resolution cryo XRF-NI elemental mapping of cells (40 nm) with quantification of iridium area density per pixel, providing an imaging platform for future studies comparing the incorporation of various reporters, or of a given reporter in different conditions. Such Ir(III) probes are thus amenable to multimodal correlative bioimaging studies, laying a foundation for further advances in glycosciences, but could also be used to monitor any other type of biomolecule accessible through bioorthogonal labeling. By addressing key challenges and opening new possibilities, such approaches are poised to play a pivotal role in advancing our understanding of complex biological processes, advocating for the continued integration of organometallic probes into the toolkit of chemical biologists.

ASSOCIATED CONTENT

Supporting Information

The supporting information is available free of charge at https://XXXX

Synthesis and analysis of chemical reporters 4-7 and probes 3a-d, photophysical characterization, validation by HPLC and in cells, procedures for cell culture, bioorthogonal labeling, imaging (LSCM, PLIM, XRF-NI) and ICP-MS analysis, supplementary figures S1-S17, supplementary table S1.

AUTHOR INFORMATION

Corresponding authors

Christophe Biot – *Univ. Lille, CNRS, UMR 8576 - UGSF - Unité de Glycobiologie Structurale et Fonctionnelle, Lille, France;* orcid.org/0000-0002-7396-1959; Email : christophe.biot@univ-lille.fr

Cédric Lion – *Univ. Lille, CNRS, UMR 8576 - UGSF - Unité de Glycobiologie Structurale et Fonctionnelle, Lille, France;* orcid.org/0000-0001-6591-4573; Phone : +33 320 43 69 08; Email : cedric.lion@univ-lille.fr

Authors

Vincent Rigolot – *Univ. Lille, CNRS, UMR 8576 - UGSF - Unité de Glycobiologie Structurale et Fonctionnelle, Lille, France*

Clémence Simon – *Univ. Lille, CNRS, UMR 8576 - UGSF - Unité de Glycobiologie Structurale et Fonctionnelle, Lille, France*

Aude Bouchet – *Univ. Lille, CNRS, UMR 8516 - LASIRe - Laboratoire Avancé de Spectroscopie pour les Interactions la Réactivité et l'Environnement, Lille, France*

Veronica Di Battista – *Department of Analytical and Material Science, BASF SE, Ludwigshafen, Germany; Department of Environmental and Resource Engineering, DTU Sustain, Technical University of Denmark, Building 115, Kgs. Lyngby, Denmark*

Dmitry Karpov – *ID16A Nano-imaging beamline, European Synchrotron Radiation Facility, Grenoble, France*

Boris Vauzeilles – *Chemical Biology Department, Université Paris-Saclay, CNRS, Institut de Chimie des Substances Naturelles, UPR 2301, 91198 Gif-sur-Yvette, France*

Michel Sliwa – *Univ. Lille, CNRS, UMR 8516 - LASIRe - Laboratoire Avancé de Spectroscopie pour les Interactions la Réactivité et l'Environnement, Lille, France*

Sylvain Bohic – *Université Grenoble Alpes, INSERM, UA 07 Synchrotron Radiation for Biomedicine (STROBE), Grenoble, France; ID16A Nano-imaging beamline, European Synchrotron Radiation Facility, Grenoble, France*

Author contributions

Notes

The authors declare no competing financial interest.

REFERENCES

(1)   Rostovtsev, V. V.; Green, L. G.; Fokin, V. V.; Sharpless, K. B. A Stepwise Huisgen Cycloaddition Process: Copper(I)-Catalyzed Regioselective "Ligation" of Azides and Terminal Alkynes. *Angew. Chem. Int. Ed.* **2002**, *41* (14), 2596–2599. https://doi.org/10.1002/1521-3773(20020715)41:14<2596::AID-ANIE2596>3.0.CO;2-4.

(2)   Agard, N. J.; Prescher, J. A.; Bertozzi, C. R. A Strain-Promoted [3 + 2] Azide−Alkyne Cycloaddition for Covalent Modification of Biomolecules in Living Systems. *J. Am. Chem. Soc.* **2004**, *126* (46), 15046–15047. https://doi.org/10.1021/ja044996f.

(3)   Blackman, M. L.; Royzen, M.; Fox, J. M. Tetrazine Ligation: Fast Bioconjugation Based on Inverse-Electron-Demand Diels−Alder Reactivity. *J. Am. Chem. Soc.* **2008**, *130* (41), 13518–13519. https://doi.org/10.1021/ja8053805.

(4)   Devaraj, N. K.; Weissleder, R.; Hilderbrand, S. A. Tetrazine-Based Cycloadditions: Application to Pretargeted Live Cell Imaging. *Bioconjug Chem* **2008**, *19* (12), 2297–2299. https://doi.org/10.1021/bc8004446.

(5)   Kayser, H.; Zeitler, R.; Kannicht, C.; Grunow, D.; Nuck, R.; Reutter, W. Biosynthesis of a Nonphysiological Sialic Acid in Different Rat Organs, Using N-Propanoyl-D-Hexosamines as Precursors. *J Biol Chem* **1992**, *267* (24), 16934–16938.

(6)   Tirrell, D. A. Hitting the Sweet Spot. *Nature* **2004**, *430* (7002), 837–837. https://doi.org/10.1038/430837a.

(7)   Laughlin, S. T.; Baskin, J. M.; Amacher, S. L.; Bertozzi, C. R. In Vivo Imaging of Membrane-Associated Glycans in Developing Zebrafish. *Science* **2008**, *320* (5876), 664–667. https://doi.org/10.1126/science.1155106.

(8)   Kufleitner, M.; Haiber, L. M.; Wittmann, V. Metabolic Glycoengineering – Exploring Glycosylation with Bioorthogonal Chemistry. *Chem. Soc. Rev.* **2023**, *52* (2), 510–535. https://doi.org/10.1039/D2CS00764A.

(9)   Nguyen, S. S.; Prescher, J. A. Developing Bioorthogonal Probes to Span a Spectrum of Reactivities. *Nat Rev Chem* **2020**, *4* (9), 476–489. https://doi.org/10.1038/s41570-020-0205-0.

(10)   *Far-Field Optical Nanoscopy | Science*. https://www-science-org.ressources-electroniques.univ-lille.fr/doi/10.1126/science.1137395 (accessed 2024-01-19).

(11)   Balzarotti, F.; Eilers, Y.; Gwosch, K. C.; Gynnå, A. H.; Westphal, V.; Stefani, F. D.; Elf, J.; Hell, S. W. Nanometer Resolution Imaging and Tracking of Fluorescent Molecules with Minimal Photon Fluxes. *Science* **2017**, *355* (6325), 606–612. https://doi.org/10.1126/science.aak9913.

(12)   Weber, M.; von der Emde, H.; Leutenegger, M.; Gunkel, P.; Sambandan, S.; Khan, T. A.; Keller-Findeisen, J.; Cordes, V. C.; Hell, S. W. MINSTED Nanoscopy Enters the Ångström Localization Range. *Nat Biotechnol* **2023**, *41* (4), 569–576. https://doi.org/10.1038/s41587-022-01519-4.

(13)   Conesa, J. J.; Carrasco, A. C.; Rodríguez-Fanjul, V.; Yang, Y.; Carrascosa, J. L.; Cloetens, P.; Pereiro, E.; Pizarro, A. M. Unambiguous Intracellular Localization and Quantification of a Potent Iridium Anticancer Compound by Correlative 3D Cryo X-Ray Imaging. *Angewandte Chemie International Edition* **2020**, *59* (3), 1270–1278. https://doi.org/10.1002/anie.201911510.

(14)   Tan, J.; Zhang, X.; Wang, X.; Xu, C.; Chang, S.; Wu, H.; Wang, T.; Liang, H.; Gao, H.; Zhou, Y.; Zhu, Y. Structural Basis of Assembly and Torque Transmission of the Bacterial Flagellar Motor. *Cell* **2021**, *184* (10), 2665-2679.e19. https://doi.org/10.1016/j.cell.2021.03.057.

(15)   Walter, A.; Paul-Gilloteaux, P.; Plochberger, B.; Sefc, L.; Verkade, P.; Mannheim, J. G.; Slezak, P.; Unterhuber, A.; Marchetti-Deschmann, M.; Ogris, M.; Bühler, K.; Fixler, D.; Geyer, S. H.; Weninger, W. J.; Glösmann, M.; Handschuh, S.; Wanek, T. Correlated Multimodal Imaging in Life Sciences: Expanding the Biomedical Horizon. *Frontiers in Physics* **2020**, *8*.

(16)   Rigolot, V.; Biot, C.; Lion, C. To View Your Biomolecule, Click inside the Cell. *Angewandte Chemie International Edition* **2021**, *60* (43), 23084–23105. https://doi.org/10.1002/anie.202101502.

(17)   Qin, W.; Qin, K.; Fan, X.; Peng, L.; Hong, W.; Zhu, Y.; Lv, P.; Du, Y.; Huang, R.; Han, M.; Cheng, B.; Liu, Y.; Zhou, W.; Wang, C.; Chen, X. Artificial Cysteine S-Glycosylation Induced by Per-O-Acetylated Unnatural Monosaccharides during Metabolic Glycan Labeling. *Angewandte Chemie International Edition* **2018**, *57* (7), 1817–1820. https://doi.org/10.1002/anie.201711710.

(18)   Chuh, K. N.; Zaro, B. W.; Piller, F.; Piller, V.; Pratt, M. R. Changes in Metabolic Chemical Reporter Structure Yield a Selective Probe of O-GlcNAc Modification. *J. Am. Chem. Soc.* **2014**, *136* (35), 12283–12295. https://doi.org/10.1021/ja504063c.

(19)   Doll, F.; Buntz, A.; Späte, A.-K.; Schart, V. F.; Timper, A.; Schrimpf, W.; Hauck, C. R.; Zumbusch, A.; Wittmann, V. Visualisierung proteinspezifischer Glycosylierung in lebenden Zellen. *Angewandte Chemie* **2016**, *128* (6), 2303–2308. https://doi.org/10.1002/ange.201503183.

(20)   Sun, Y.; Hong, S.; Xie, R.; Huang, R.; Lei, R.; Cheng, B.; Sun, D.-E.; Du, Y.; Nycholat, C. M.; Paulson, J. C.; Chen, X. Mechanistic Investigation and Multiplexing of Liposome-Assisted Metabolic Glycan Labeling. *J Am Chem Soc* **2018**, *140* (10), 3592–3602. https://doi.org/10.1021/jacs.7b10990.

(21)   Qin, K.; Zhang, H.; Zhao, Z.; Chen, X. Protein S-Glyco-Modification through an Elimination–Addition Mechanism. *J. Am. Chem. Soc.* **2020**, *142* (20), 9382–9388. https://doi.org/10.1021/jacs.0c02110.

(22)   Wang, F.; Zhang, Y.; Liu, Z.; Du, Z.; Zhang, L.; Ren, J.; Qu, X. A Biocompatible Heterogeneous MOF–Cu Catalyst for In Vivo Drug Synthesis in Targeted Subcellular Organelles. *Angewandte Chemie International Edition* **2019**, *58* (21), 6987–6992. https://doi.org/10.1002/anie.201901760.

(23)   You, Y.; Cao, F.; Zhao, Y.; Deng, Q.; Sang, Y.; Li, Y.; Dong, K.; Ren, J.; Qu, X. Near-Infrared Light Dual-Promoted Heterogeneous Copper Nanocatalyst for Highly Efficient Bioorthogonal Chemistry in Vivo. *ACS Nano* **2020**, *14* (4), 4178–4187. https://doi.org/10.1021/acsnano.9b08949.

(24)   Deb, T.; Tu, J.; Franzini, R. M. Mechanisms and Substituent Effects of Metal-Free Bioorthogonal Reactions. *Chem Rev* **2021**, *121* (12), 6850–6914. https://doi.org/10.1021/acs.chemrev.0c01013.

(25)   Usama, S. M.; Inagaki, F.; Kobayashi, H.; Schnermann, M. J. Norcyanine-Carbamates Are Versatile Near-Infrared Fluorogenic Probes. *J. Am. Chem. Soc.* **2021**, *143* (15), 5674–5679. https://doi.org/10.1021/jacs.1c02112.

(26)   Cai, L.-J.; Wang, X.; Zong, Q.-S.; Jiang, X.-P.; Hu, H.-Y. Accessing a Long-Fluorescence-Lifetime BODIPY Dye via Efficient Förster Resonance Energy Transfer Induced by Host-Guest Doping. *ChemPhotoChem* **2023**, *7* (10), e202300042. https://doi.org/10.1002/cptc.202300042.

(27)   Wu, L.; Huang, C.; Emery, B. P.; Sedgwick, A. C.; Bull, S. D.; He, X.-P.; Tian, H.; Yoon, J.; Sessler, J. L.; James, T. D. Förster Resonance Energy Transfer (FRET)-Based Small-Molecule Sensors and Imaging Agents. *Chem. Soc. Rev.* **2020**, *49* (15), 5110–5139. https://doi.org/10.1039/C9CS00318E.

(28)   Zeng, S.; Liu, X.; Kafuti, Y. S.; Kim, H.; Wang, J.; Peng, X.; Li, H.; Yoon, J. Fluorescent Dyes Based on Rhodamine Derivatives for Bioimaging and Therapeutics: Recent Progress, Challenges, and Prospects. *Chem. Soc. Rev.* **2023**, *52* (16), 5607–5651. https://doi.org/10.1039/D2CS00799A.

(29)   Lo, K. K.-W.; Li, S. P.-Y.; Zhang, K. Y. Development of Luminescent Iridium(III) Polypyridine Complexes as Chemical and Biological Probes. *New J. Chem.* **2011**, *35* (2), 265–287. https://doi.org/10.1039/C0NJ00478B.

(30)   Baggaley, E.; Weinstein, J. A.; Williams, J. A. G. Lighting the Way to See inside the Live Cell with Luminescent Transition Metal Complexes. *Coordination Chemistry Reviews* **2012**, *256* (15), 1762–1785. https://doi.org/10.1016/j.ccr.2012.03.018.

(31)   Zhao, Q.; Huang, C.; Li, F. Phosphorescent Heavy-Metal Complexes for Bioimaging. *Chemical Society Reviews* **2011**, *40* (5), 2508–2524. https://doi.org/10.1039/C0CS00114G.

(32)   Murphy, L.; Congreve, A.; Pålsson, L.-O.; Williams, J. A. G. The Time Domain in Co-Stained Cell Imaging: Time-Resolved Emission Imaging Microscopy Using a Protonatable Luminescent Iridium Complex. *Chem. Commun.* **2009**, *46* (46), 8743–8745. https://doi.org/10.1039/C0CC03705B.

(33)   Lee, L. C.-C.; Lo, K. K.-W. Luminescent and Photofunctional Transition Metal Complexes: From Molecular Design to Diagnostic and Therapeutic Applications. *J. Am. Chem. Soc.* **2022**, *144* (32), 14420–14440. https://doi.org/10.1021/jacs.2c03437.

(34)   Lo, K. K.-W.; Chan, B. T.-N.; Liu, H.-W.; Zhang, K. Y.; Li, S. P.-Y.; Tang, T. S.-M. Cyclometalated Iridium(III) Polypyridine Dibenzocyclooctyne Complexes as the First Phosphorescent Bioorthogonal Probes. *Chem. Commun.* **2013**, *49* (39), 4271–4273. https://doi.org/10.1039/C2CC36907A.

(35)   Li, S. P.-Y.; Yip, A. M.-H.; Liu, H.-W.; Lo, K. K.-W. Installing an Additional Emission Quenching Pathway in the Design of Iridium(III)-Based Phosphorogenic Biomaterials for Bioorthogonal Labelling and Imaging. *Biomaterials* **2016**, *103*, 305–313. https://doi.org/10.1016/j.biomaterials.2016.06.065.

(36)   Tang, T. S.-M.; Liu, H.-W.; Lo, K. K.-W. Monochromophoric Iridium(III) Pyridyl–Tetrazine Complexes as a Unique Design Strategy for Bioorthogonal Probes with Luminogenic Behavior. *Chem. Commun.* **2017**, *53* (23), 3299–3302. https://doi.org/10.1039/C7CC00427C.

(37)   Yip, A. M.-H.; Lai, C. K.-H.; Yiu, K. S.-M.; Lo, K. K.-W. Phosphorogenic Iridium(III) Bis-Tetrazine Complexes for Bioorthogonal Peptide Stapling, Bioimaging, Photocytotoxic Applications, and the Construction of Nanosized Hydrogels. *Angewandte Chemie International Edition* **2022**, *61* (16), e202116078. https://doi.org/10.1002/anie.202116078.

(38)   Wang, J.; Xue, J.; Yan, Z.; Zhang, S.; Qiao, J.; Zhang, X. Photoluminescence Lifetime Imaging of Synthesized Proteins in Living Cells Using an Iridium–Alkyne Probe. *Angewandte Chemie International Edition* **2017**, *56* (47), 14928–14932. https://doi.org/10.1002/anie.201708566.

(39)   Wu, Q.; Zhang, K. Y.; Dai, P.; Zhu, H.; Wang, Y.; Song, L.; Wang, L.; Liu, S.; Zhao, Q.; Huang, W. Bioorthogonal "Labeling after Recognition" Affording an FRET-Based Luminescent Probe for Detecting and Imaging Caspase-3 via Photoluminescence Lifetime Imaging. *J. Am. Chem. Soc.* **2020**, *142* (2), 1057–1064. https://doi.org/10.1021/jacs.9b12191.

(40)   Ma, D.-L.; He, H.-Z.; Leung, K.-H.; Chan, D. S.-H.; Leung, C.-H. Bioactive Luminescent Transition-Metal Complexes for Biomedical Applications. *Angewandte Chemie International Edition* **2013**, *52* (30), 7666–7682. https://doi.org/10.1002/anie.201208414.

(41)   Liu, C.; Yang, C.; Lu, L.; Wang, W.; Tan, W.; Leung, C.-H.; Ma, D.-L. Luminescent Iridium(III) Complexes as COX-2-Specific Imaging Agents in Cancer Cells. *Chem. Commun.* **2017**, *53* (19), 2822–2825. https://doi.org/10.1039/C6CC08109F.

(42)   Vellaisamy, K.; Li, G.; Ko, C.-N.; Zhong, H.-J.; Fatima, S.; Kwan, H.-Y.; Wong, C.-Y.; Kwong, W.-J.; Tan, W.; Leung, C.-H.; Ma, D.-L. Cell Imaging of Dopamine Receptor Using Agonist Labeling Iridium(III) Complex. *Chem. Sci.* **2018**, *9* (5), 1119–1125. https://doi.org/10.1039/C7SC04798C.

(43)   Würth, C.; Grabolle, M.; Pauli, J.; Spieles, M.; Resch-Genger, U. Relative and Absolute Determination of Fluorescence Quantum Yields of Transparent Samples. *Nat Protoc* **2013**, *8* (8), 1535–1550. https://doi.org/10.1038/nprot.2013.087.

(44)   Zhang, K. Y.; Liu, H.-W.; Fong, T. T.-H.; Chen, X.-G.; Lo, K. K.-W. Luminescent Dendritic Cyclometalated Iridium(III) Polypyridine Complexes: Synthesis, Emission Behavior, and Biological Properties. *Inorg. Chem.* **2010**, *49* (12), 5432–5443. https://doi.org/10.1021/ic902443e.

(45)   Solomatina, A. I.; Su, S.-H.; Lukina, M. M.; Dudenkova, V. V.; Shcheslavskiy, V. I.; Wu, C.-H.; Chelushkin, P. S.; Chou, P.-T.; Koshevoy, I. O.; Tunik, S. P. Water-Soluble Cyclometalated Platinum(II) and Iridium(III) Complexes: Synthesis, Tuning of the Photophysical Properties, and in Vitro and in Vivo Phosphorescence Lifetime Imaging. *RSC Adv.* **2018**, *8* (31), 17224–17236. https://doi.org/10.1039/C8RA02742K.

(46)   Gilormini, P. A.; Lion, C.; Vicogne, D.; Levade, T.; Potelle, S.; Mariller, C.; Guérardel, Y.; Biot, C.; Foulquier, F. A Sequential Bioorthogonal Dual Strategy: ManNAl and SiaNAl as Distinct Tools to Unravel Sialic Acid Metabolic Pathways. *Chem. Commun.* **2016**, *52* (11), 2318–2321. https://doi.org/10.1039/C5CC08838K.

(47)   Gilormini, P. A.; Lion, C.; Vicogne, D.; Guérardel, Y.; Foulquier, F.; Biot, C. Chemical Glycomics Enrichment: Imaging the Recycling of Sialic Acid in Living Cells. *J Inherit Metab Dis* **2018**, *41* (3), 515–523. https://doi.org/10.1007/s10545-017-0118-3.

(48)   Estandarte, A. K.; Botchway, S.; Lynch, C.; Yusuf, M.; Robinson, I. The Use of DAPI Fluorescence Lifetime Imaging for Investigating Chromatin Condensation in Human Chromosomes. *Sci Rep* **2016**, *6* (1), 31417. https://doi.org/10.1038/srep31417.

(49)   Domart, F.; Cloetens, P.; Roudeau, S.; Carmona, A.; Verdier, E.; Choquet, D.; Ortega, R. Correlating STED and Synchrotron XRF Nano-Imaging Unveils Cosegregation of Metals and Cytoskeleton Proteins in Dendrites. *eLife* **2020**, *9*, e62334. https://doi.org/10.7554/eLife.62334.

(50)   Rodushkin, I.; Engström, E.; Stenberg, A.; Baxter, D. C. Determination of Low-Abundance Elements at Ultra-Trace Levels in Urine and Serum by Inductively Coupled Plasma-Sector Field Mass Spectrometry. *Anal Bioanal Chem* **2004**, *380* (2), 247–257. https://doi.org/10.1007/s00216-004-2742-7.

(51)   Fus, F.; Yang, Y.; Lee, H. Z. S.; Top, S.; Carriere, M.; Bouron, A.; Pacureanu, A.; da Silva, J. C.; Salmain, M.; Vessières, A.; Cloetens, P.; Jaouen, G.; Bohic, S. Intracellular Localization of an Osmocenyl-Tamoxifen Derivative in Breast Cancer Cells Revealed by Synchrotron Radiation X-Ray Fluorescence Nanoimaging. *Angew Chem Int Ed Engl* **2019**, *58* (11), 3461–3465. https://doi.org/10.1002/anie.201812336.

(52)   Bissardon, C.; Reymond, S.; Salomé, M.; André, L.; Bayat, S.; Cloetens, P.; Bohic, S. Cell Culture on Silicon Nitride Membranes and Cryopreparation for Synchrotron X-Ray Fluorescence Nano-Analysis. *J Vis Exp* **2019**, No. 154. https://doi.org/10.3791/60461.

(53)   Gramaccioni, C.; Yang, Y.; Pacureanu, A.; Vigano, N.; Procopio, A.; Valenti, P.; Rosa, L.; Berlutti, F.; Bohic, S.; Cloetens, P. Cryo-Nanoimaging of Single Human Macrophage Cells: 3D Structural and Chemical Quantification. *Anal. Chem.* **2020**, *92* (7), 4814–4819. https://doi.org/10.1021/acs.analchem.9b04096.